Journal of Materials Chemistry C

Accepted Manuscript

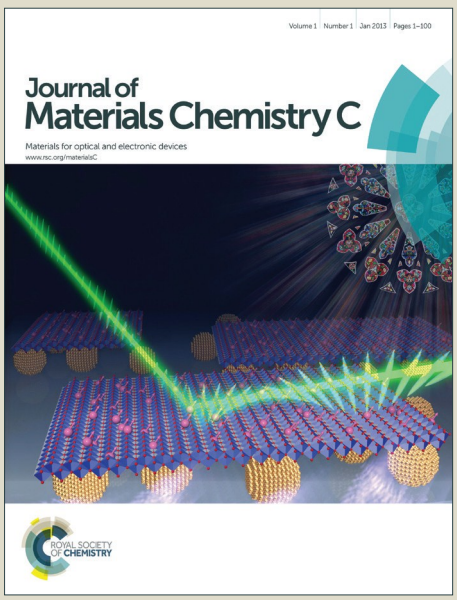

ROYAL SOCIETY OF CHEMISTRY

www.rsc.org/materialsC

Journal of Material Chemistry C

Cite this: DOI: 10.1039/c0xx00000x

ARTICLE

www.rsc.org/xxxxxx

Tunable luminescence and energy transfer properties in $Ca_8MgLu(PO_4)_7:Ce^{3+},Tb^{3+}, Mn^{2+}$ phosphors

Xiaoyun Mi[a,b], Jiacheng Sun[b], Peng Zhou[b], Hongyan Zhou[b], Di Song[b], Kai Li[a], Mengmeng Shang*[a], Lin Jun*[a]

Received (in XXX, XXX) Xth XXXXXXXXX 20XX, Accepted Xth XXXXXXXXX 20XX
DOI: 10.1039/b000000x

The $Ca_8MgLu(PO_4)_7:Ce^{3+}$, Tb^{3+}, Mn^{2+} (abbreviated as CMLP:Ce^{3+}, Tb^{3+}, Mn^{2+}) phosphors have been synthesized by high temperature solid state method. X-ray diffraction (XRD), photoluminescence (PL) spectra, GSAS structure refinement, absolute quantum yield and lifetimes were utilized to characterize the samples. With increasing Ce^{3+} doping concentration in the CMLP host, the emission peak has a red shift from 360 nm to 374 nm. Under UV excitation, both of the energy transfers (ETs) from Ce^{3+} to Tb^{3+} and from Ce^{3+} to Mn^{2+} in the CMLP host have been demonstrated to be resonant type via a dipole-quadrupole mechanism, and the critical distance (R_C) were calculated by the quenching concentration method and spectral overlap method, respectively. The emitting colors of CMLP:Ce^{3+}, Tb^{3+}, Mn^{2+} samples can be adjusted from blue to green, eventually to orange-red by ET mechanisms between Ce^{3+} and Tb^{3+}/Mn^{2+}. Moreover, a wide-range-tunable white light emission with absolute quantum yields of 50% were obtained by precisely controlling the contents of Ce^{3+}, Tb^{3+} and Mn^{2+} ions. Temperature dependence luminescence spectra prove the good thermal stability of as-prepared phosphor. Based on the good PL properties and varied hues of the CMLP host by adjusting the doping concentration of the activators (Ce^{3+}, Tb^{3+}, Mn^{2+}), CMLP might be promising as a host material for using in solid-state lighting and display fields.

1. Introduction

With the performances of white light-emitting diodes (w-LEDs) promoting, w-LEDs have drawn much attention in the lighting market against the current background of global energy shortages[1,2] due to the merits of environmental friendliness, energy saving, high brightness and long lifetime.[3,4] At present, commercial w-LEDs are mainly realized by combining a GaN-based blue LED chip with $Y_3Al_5O_{12}:Ce^{3+}$ (YAG: Ce) yellow phosphor. Since the emission spectrum of YAG: Ce is short of red component, the obtained LEDs cannot meet the requirements for indoor lighting which needs warm white light and excellent color rendering.[5,6,7] In order to overcome the disadvantage of this combination, researchers begin to combine (near) ultraviolet LED chip with blue, green and red tri-color phosphors to generate white light. Generally, the luminescent efficiency is relatively low in this system owing to the strong reabsorption of the blue light by the red and green phosphors.[8] These short comings prevent the use of LEDs in general lighting applications, so the single-phase white-emitting phosphors are required for UV-pumped w-LEDs to improve the luminescence reproducibility and efficiency.[9,10]

Phosphates as the hosts for the phosphor materials have the advantages of low synthetic cost, relatively simple tech-process, outstanding thermal stability and the strong adsorption band in the (near) ultraviolet region.[11,12] In the recent years, researchers have developed some single-component phosphate phosphors with color-tunable white-light-emitting for application in UV-excited white LED.[9-12] The whitlockite-type β-$Ca_3(PO_4)_2$ compound, as a typical phosphate, has six metal sites (M1–6) in the crystal lattice: the M1–M2 sites are coordinated by eight oxygen atoms, the M3 and M5 sites are surrounded by nine and six oxygen atoms, and the M4, M6 sites is vacant.[13,14] The presence of this particular structure suggests a possible method by which the lattice can accommodate other cations with similar radii and charges without significant changes to the structural frame. So far, some $Ca_3(PO_4)_2$-type luminescence materials, such as $Ca_8MgR(PO_4)_7:Eu^{3+}$(R=La, Gd, Y), $Ca_8MgGd(PO_4)_7:Eu^{2+}$, and $Ca_8MgLa(PO_4)_7:Ce^{3+}$, Mn^{2+} have been studied by many researchers.[15-18] However, Ce^{3+}, Tb^{3+} and Mn^{2+} activated $Ca_8MgLu(PO_4)_7$ (abbreviated as CMLP) phosphors realizing white light emission and the energy transfer (ET) processes of $Ce^{3+}\rightarrow Tb^{3+}$, $Ce^{3+}\rightarrow Mn^{2+}$, and $Tb^{3+}\rightarrow Mn^{2+}$ have rarely been reported.

In the present work, we choose CMLP as the host material and investigate the luminescence properties of Ce^{3+}, Tb^{3+} and/or Mn^{2+} activated CMLP samples in detail. Three kinds of Ce^{3+} sites in the CMLP host are ascertained via GSAS structure refinement method. The thermostability properties of as-prepared CMLP: Ce^{3+}, Tb^{3+}, Mn^{2+} sample and the energy transfer mechanism of the $Ce^{3+}\rightarrow Tb^{3+}$ and $Ce^{3+}\rightarrow Mn^{2+}$ ion pairs in the CMLP were also researched. The corresponding critical distance (R_C) was calculated by the quenching concentration method and spectral

overlap method, respectively. This work can provide some reference for developing phosphors which can be excited effectively by ultraviolet/near ultraviolet w-LED.

2. Experimental

2.1 Materials

CeO_2 and Tb_4O_7 (99.999%) were purchased from Science and Technology Parent Company of Changchun Institute of Applied Chemistry and all other chemicals were purchased from Beijing Chemical Company. All chemicals were analytical grade reagents and were used directly without further purification.

2.2 Preparation

A series of polycrystalline $Ca_8MgLu(PO_4)_7$(CMLP) and different concentrations of Ce^{3+}, Tb^{3+}, Mn^{2+} ion-doped CMLP powder samples were prepared by a conventional high temperature solid state reaction process. Typically, stoichiometric amounts of $CaCO_3$ (A.R), $MgCO_3$ (A.R), $MnCO_3$ (A.R), $NH_4H_2PO_4$ (A.R), Y_2O_3 (99.99%), La_2O_3 (99.99%), Gd_2O_3 (99.99%), Lu_2O_3 (99.99%), CeO_2 (99.99%), Tb_4O_7 (99.99%) and Eu_2O_3 (99.99%) were thoroughly mixed in an agate mortar for 1h with an appropriate amount of ethanol and then dried at 90 ^{0}C. The powder mixtures were sintered at 1200 ^{0}C for 4h in 5%H_2-95%N_2 reducing atmosphere to produce the final samples.

2.3 Characterization

Powder X-ray diffraction (XRD) patterns were collected by using Cu Kα radiation (λ = 1.54056 Å) on a RigakuD/max-II B diffractometer, operating at 40 kV and 40 mA. The structure refinement was done using the General Structure Analysis System (GSAS) program.[19] The surface morphology of the film was analyzed by a Hitachi S4200 Scanning Electron Microscopy (SEM). The photoluminescence (PL) measurements were performed on a Hitachi F-7000 spectrophotometer equipped with a 150W xenon lamp as the excitation source. The temperature-dependent (300-500K) PL spectra were obtained on a fluorescence spectrophotometer equipped with a 450W xenon lamp as the excitation source (Edinburgh Instruments, FLSP-920) with a temperature controller. Photoluminescence absolute quantum yields (QYs) were measured by an absolute PL quantum yield measurement system (C9920-02, Hamamatsu Photonics K. K., Japan). The luminescence decay curves were obtained from a Lecroy Wave Runner 6100 digital oscilloscope (1GHz) using a tunable laser (pulse width = 4 ns, gate = 50 ns) as the excitation (Contimuum Sunlite OPO) source. All the measurements were performed at room temperature (RT).

3. Results and discussion

3.1 Crystallization behaviour and structure

CMLP belonging to the family of pyrophosphorite compounds, has the similar structure to β-$Ca_3(PO_4)_2$ with no inversion symmetry.[13,14,20] In the structure of CMLP, there are six different metal cations crystallographic sites M(1)-M(6) and the M(4)/M(6) sites are vacant sites. The M(1), M(2), M(3), M(5) positions are coordinated with eight, eight, nine and six oxygen atoms, respectively.[21,22] Mg^{2+} (0.73Å) ion occupies the site M(5) of Ca^{2+} (1.00 Å) ion on account of small radius,[23,24] so the coordination number of Mg^{2+} in the CMLP compound is 6. Figure 1 shows the representative XRD patterns of different RE^{3+} ions activated samples annealed at 1200 ^{0}C for 4 h in H_2/N_2 (5%/95%). It is obvious that all the diffraction peaks of these samples can be exactly assigned to the pure host structure with JCPDS card no. 46-0409, indicating that the obtained samples are single phase and the doped Ce^{3+}, Tb^{3+} and Mn^{2+} ions do not cause any significant change in the host structure.

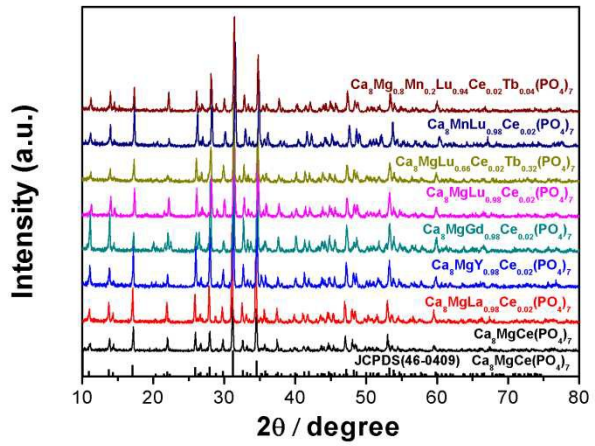

Figure 1. The representative XRD patterns of the sample.

In order to determine the structure of the obtained phosphor, rietveld structure refinement for the $Ca_8MgCe(PO_4)_7$ compound was performed using the powder diffraction data. The experimental, calculated, and diffraction XRD profiles for the $Ca_8MgCe(PO_4)_7$ annealed at 1200 ^{0}C for 4h in H_2/N_2 (5%/95%) are shown in Figure 2a. The starting model was built with crystallographic data taken from the structure of $Ca_9La(PO_4)_7$ (ICSD-83401) and the crystal structure of $Ca_8MgCe(PO_4)_7$ is identical with that of $Ca_9La(PO_4)_7$.[13,14,20] It is supposed that Ca^{2+} ions locating at M(5) are replaced by Mg^{2+} ions. From Figure 2a and Table 1, it is observed that experimental data is consistent with calculating data. The pure $Ca_8MgCe(PO_4)_7$ crystallizes trigonally with space group R3c (No.161) with a = b = 10.402 Å, c = 37.106 Å, V = 3498.832 Å^3, α = β = 90^0, γ =120^0. All atom positions, occupation probability, and temperature factor were refined by convergence and satisfied well the reflection conditions, R_p = 4.08%, R_{wp} = 5.3%, χ^2 = 2.573. Structure parameters for $Ca_8MgCe(PO_4)_7$ as determined by rietveld refinement of powder XRD data is identical with its real situation. The crystal structure of $Ca_8MgCe(PO_4)_7$ and the coordinated condition of Ca1(Ce1)(18b), Ca2(Ce2)(18b), Ca3(Ce3)(18b) and Mg(6a), which are coordinated by 8, 8, 9, and 6 atoms, are presented in Figure 2b. Therefore, coordination environments for the two crystallographic sites of Ca^{2+} ions in the host are ascertained in the $Ca_8MgCe(PO_4)_7$ host: eight and nine coordination centers. The morphology of the $Ca_8MgCe(PO_4)_7$ sample prepared by solid-state reaction is presented in Figure 2c. The powder consists of well-dispersed particles with particle sizes of 9 μm.

3.2 Photoluminescence and energy transfer properties in CMLP: Ce^{3+}, Mn^{2+}, Tb^{3+}

3.2.1 Photoluminescence properties of CMLP: Ce^{3+}

Figure 3 shows the excitation spectrum, emission spectrum and energy level splitting of CMLP:0.02Ce^{3+}. Under UV excitation

Table 1. Structure parameters for $Ca_8MgCe(PO_4)_7$ as determined by rietveld refinement of powder XRD data at room temperature.

Atom	Wyck	x	y	z	Occupancy
Ca1	18b	0.712	0.854	0.432	0.986
Ce1	18b	0.712	0.854	0.432	0.014
Ca2	18b	0.620	0.794	0.230	0.958
Ce2	18b	0.620	0.794	0.230	0.042
Ca3	18b	0.134	0.270	0.326	0.889
Ce3	18b	0.134	0.270	0.326	0.111
Mg	6a	0	0	0	1
P1	6a	0	0	0.265	1
P2	18b	0.687	0.856	0.134	1
P3	18b	0.657	0.852	0.032	1
O1	6a	0	0	0.307	1
O2	18b	0.051	0.970	0.253	1
O3	18b	0.746	0.842	0.174	1
O4	18b	0.676	0.835	0.130	1
O5	18b	0.732	0.997	0.112	1
O6	18b	0.481	0.728	0.131	1
O7	18b	0.581	0.899	0.045	1
O8	18b	0.623	0.726	0.043	1
O9	18b	0.808	0.920	0.035	1
O10	18b	0.641	0.808	0.996	1

*Symmetry: hexagonal, space group: $P6_3/m$, z=6, a=b=10.402Å, c=37.106Å, V=3498.832Å^3, α=β=90^0, γ=120^0. R_p=4.08%, R_{wp}=5.3%, χ^2 =2.573

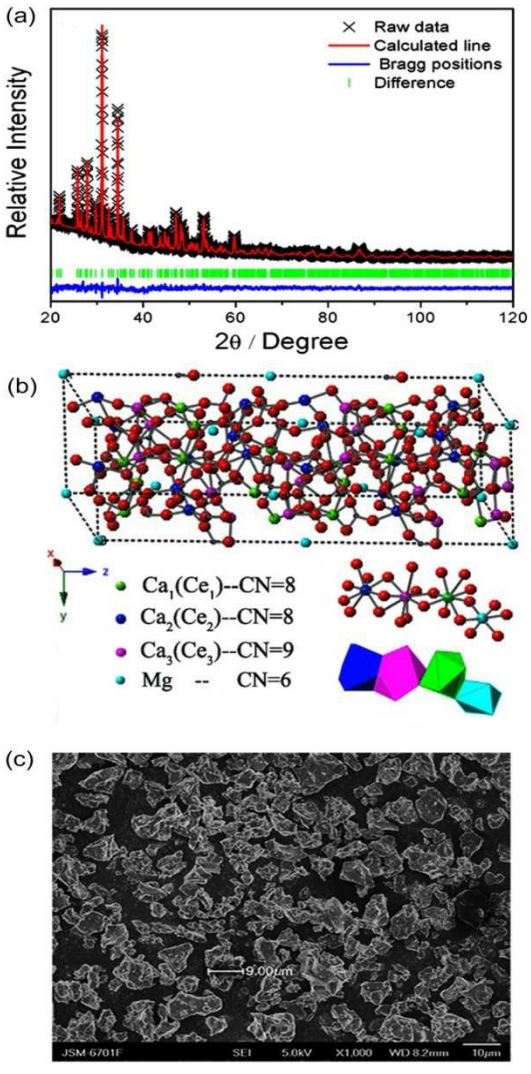

Figure 2. Rietveld refinement of the powder XRD pattern of $Ca_8MgCe(PO_4)_7$ (a), the crystal structure of sample and coordination condition of Ca^{2+} and Ce^{3+} (b), the SEM (c).

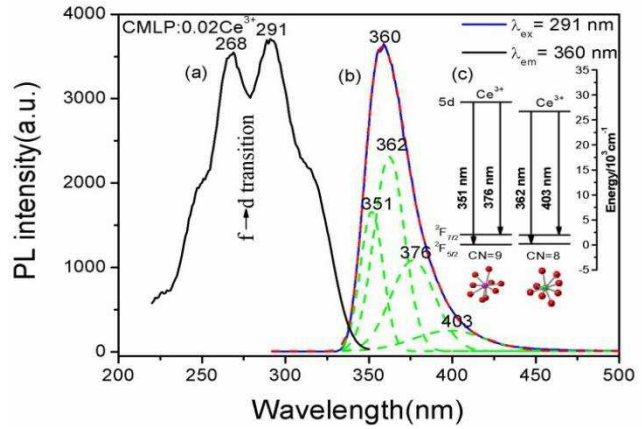

Figure 3. Excitation spectrum (a), emission spectrum (b) and the diagram for energy level splitting (c) of CMLP:0.02Ce^{3+}.

of 291 nm, the emission spectrum of the CMLP:0.02Ce^{3+} sample displays an asymmetric broad emission band that ranges from 320 to 450 nm with a maximum at about 360 nm. Generally, the Ce^{3+} emission spectrum has doublet character because of the spin −orbit splitting of the ground state ($^2F_{5/2}$ and $^2F_{7/2}$) with an energy difference of about 2000 cm^{-1}.[5,25] Although the Ce^{3+} emission spectrum is one band, any disorder and/or charge compensation can change the local environment around specific Ce^{3+} ions, thereby modifying the position of the 4f → 5d transition. Many references have specified the Ce^{3+} sites by using the method of decomposing its excitation and emission spectra.[26,27,28] In the CMLP:0.02Ce^{3+} sample, the emission band of Ce^{3+} ions consists of four well-separated Gaussian components with peak centering at 351, 362, 376 and 403 nm, as shown in curve b in Figure 3. The energy difference between 351nm and 376 nm is about 1890 cm^{-1}, which can be assigned to the splitting of the 4f ground state ($^2F_{5/2}$ and $^2F_{7/2}$). However, the energy difference between 362 and 403 nm in the CMLP host is about 2810 cm^{-1}, which is far from 2000 cm^{-1}. Therefore, these four peaks can arise from not only the ground state splitting but also the different locations of Ce^{3+}. The coordination environments for the two crystallographic sites of Ca^{2+} ions in the CMLP host calculated by the Van Uitert

formula: eight and nine coordination centers. Figure 3a and c display the energy level diagrams of Ce^{3+} at the two different coordination fields. From the van Uitert formula and the energy level diagrams, there is a strong correlation between the emitting position of Ce^{3+} ions and coordination environments.

The relationship between the emitting energy of Ce^{3+} ions and local structure of different compounds can be fitted successfully based on the following equation:[26]

$$E(cm^{-1}) = Q^*\left[1-\left(\frac{V}{4}\right)^{\frac{1}{V}}\times 10^{\frac{-(n\times Ea\times r)}{80}}\right] \qquad (1)$$

E represents the emission peak sites of Ce^{3+} ions; Q^* represents the energy position having a lower d energy band of free Ce^{3+} ions ($Q^* = 50000\ cm^{-1}$), V is the valence of Ce^{3+} ions ($V = 3$), n is the number of anionic in the shell lying closest to Ce^{3+}, Ea is electron affinities of atom in the process of forming anion (eV), r represents the radius of cation ionic replaced by Ce^{3+} ions in the host (Å). In the same base material, Ea is constant, $V = 3$, $Q^* = 50000\ cm^{-1}$. Previous literature showed that the radius of eight-coordinated centers and nine-coordinated center are 112, 118 pm,[20] respectively. From the van Uitert formula (1) and the figure of energy level splitting 3c, we can conclude that the two bands centering at 351 and 376 nm (energy difference is about 1890 cm^{-1}) are attributed to the Ce^{3+} ions entering the nine-coordinated center, and the two bands located at 362 and 403 nm (energy difference is about 2810 cm^{-1}) are due to the emission of Ce^{3+} ions occupying the eight coordinated center.[27] The 4f orbits of Y^{3+}, La^{3+}, Gd^{3+}, and Lu^{3+} are half-filled, full-filled or empty. Thus these ions don't have fluorescence emission. The influence of Y^{3+}, La^{3+}, Gd^{3+}, and Lu^{3+} on luminescence properties of $Ca_8MgM(PO_4)_7$ is shown in Figure 4a.

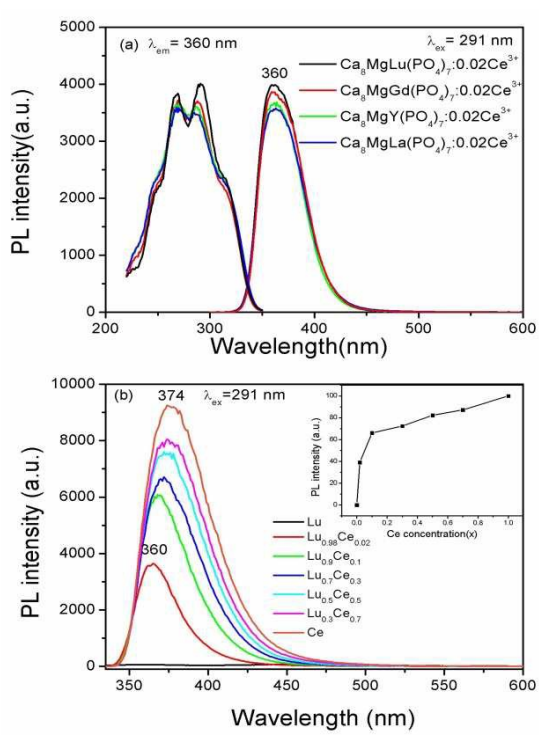

Figure 4. Various excitation and emission spectra of the $Ca_8MgLn(PO_4)_7$ (Ln=Y^{3+}, La^{3+}, Gd^{3+}, Lu^{3+}) phosphors with different doping rare earth (a) and different Ce^{3+} doping concentrations (b).

With doping Ln^{3+} (Y^{3+}, La^{3+}, Gd^{3+}, Lu^{3+}) ions, the locations of main peaks in emission spectrum do not change obviously. The luminous intensity of Ce^{3+} ions increases gradually, due to radius of Ln^{3+} ions decreasing ($r_{La^{3+}} > r_{Ce^{3+}} > r_{Gd^{3+}} > r_{Y^{3+}} > r_{Lu^{3+}}$).[31,32,33] Due to a mass of M(4) and M(6) vacancy existing in the structure of CMLP, the distance of luminescence center Ce^{3+} ions is enlarged. Therefore, decreasing radii of Ln^{3+} ions leads to the $Ca_8MgGd(PO_4)_7:Ce^{3+}$ is stronger than that of $Ca_8MgY(PO_4)_7:Ce^{3+}$ due to the fact that Gd^{3+} can transfer its energy to Ce^{3+} ions in the $Ca_8MgGd(PO_4)_7$ host.[29,30] It is well known that the Gd^{3+} ions has $4f^7$ electron configuration, with ground state $^8S_{7/2}$, and excited states such as ^6P, ^6I, ^6D etc. Its excitation and emission peaks are located at UV region, such as 276 nm (^6I-$^8S_{7/2}$) and 314 nm (^6P-$^8S_{7/2}$), respectively. In $Ca_8MgGd(PO_4)_7$ host, the luminescence of doped Ce^{3+} ions predominates, because the photoluminescence of induced Ce^{3+} ions emits strongly which covers the luminescence of Gd^{3+} ions.

Figure 4b shows emission spectra of the CMLP with different Ce^{3+} doping concentrations. With the concentration of Ce^{3+} increasing, the luminescent intensity gradually increases. When Ce^{3+} ions replace Lu^{3+} completely, photoluminescence intensity of the phosphor reaches the maximum. Meanwhile, the emission band shows red-shifted with an increase in the doping concentration of Ce^{3+} ions, since the Ce^{3+} ions have smaller electronegativity than Lu^{3+} ions and the covalent bond energy of Ce-O is less than that of Lu-O. When concentration of Lu^{3+} ions is large enough, it can adsorb more O^{2-} ions around itself and Ce^{3+} ions whose centroid displacement of 5d energy level decreases and the level position of lowest excited state elevates are much closer to freedom. As a result, the emission band of Ce^{3+} ions shows a blue shift. With concentration of Ce^{3+} ions increasing, the number of Lu-O bond and the level position of lowest excited state decreases, while the influence of O^{2-} ions impacting on Ce^{3+} whose centroid displacement of 5d energy level increases. As a result, the emission band of Ce^{3+} ions shows a red shift.[34,35] No concentration quenching effect of Ce^{3+} in $Ca_8MgLu(PO_4)_7$ was observed in the experiment, and this can be explained by the specific of the crystal structure of the host matrix. The $Ca_8MgLu(PO_4)_7$ belongs to the typical whitlockite structure with space group of $R3c$. In the structure of $Ca_8MgLu(PO_4)_7$, there are six different sites for Ca^{2+}, named as M(1)-M(6). Among the six sites, M(6) and M(4) site are completely empty. This chemical formula can be expressed as $Ca_8Lu(1,2,3)\square(4)Mg(5)\square(6)(PO_4)_7$ ($Z = 6$). The empty M(4) and M(6) sites can dilute the concentration of Ce^{3+}, as results of which, no concentration quenching effect is observed. In these 72 sites per unit cell, Ca^{2+} occupied 66.7%, holes occupied 16.7%, Lu^{3+} and Mg^{2+} occupied 8.3%, respectively, which means that the actual doping ratio of Ce^{3+} is 8.3% at most. We think this value is still below the empirical concentration quenching threshold of Ce^{3+}.

3.2.2 Photoluminescence properties and energy transfer in CMLP: Ce^{3+}, Tb^{3+} materials

Generally, with a low doping concentration of Tb^{3+} in the host matrix, the transitions of $^5D_3$ to ^7F_j dominate and produce blue emissions; As the Tb^{3+} concentration increases, the cross

relaxation between $^5D_3$ and $^5D_4$ occurs owing to the interaction between Tb^{3+} ions, which enhances the $^5D_4 \rightarrow {}^7F_j$ transitions with the emission color shifting from blue to green gradually.[36] Figure 5 shows the excitation spectrum and emission spectrum of CMLP:0.32Tb^{3+} sample. The excitation spectrum of CMLP:0.32Tb^{3+} sample shows a strong broad absorption band (λ_{max} = 226 nm) with shoulders at 265 , 285 nm and some weak narrow absorption peaks from 300 to 500 nm, which are due to a allowed $4f^8 \rightarrow 4f^7 5d$ transition and the intra-(4f) transitions of Tb^{3+} ions, respectively. The shoulder of the former may be due to the forbidden component of the $4f^8 \rightarrow 4f^7 5d$ transition.[37] As mentioned in the emission spectrum, CMLP:0.32Tb^{3+} can be efficiently excited by 226 nm UV and show green emission. The emission spectrum includes $^5D_{3,4} \rightarrow {}^7F_j$ transition of Tb^{3+} ions, namely $^5D_3 \rightarrow {}^7F_6$ (385 nm), $^5D_3 \rightarrow {}^7F_5$ (416 nm), $^5D_3 \rightarrow {}^7F_4$ (438 nm), $^5D_3 \rightarrow {}^7F_3$ (458 nm), $^5D_3 \rightarrow {}^7F_2$ (475 nm), $^5D_4 \rightarrow {}^7F_6$ (492 nm), $^5D_4 \rightarrow {}^7F_5$ (545 nm), $^5D_4 \rightarrow {}^7F_4$ (586 nm), and $^5D_4 \rightarrow {}^7F_3$ (622 nm).[37,38]

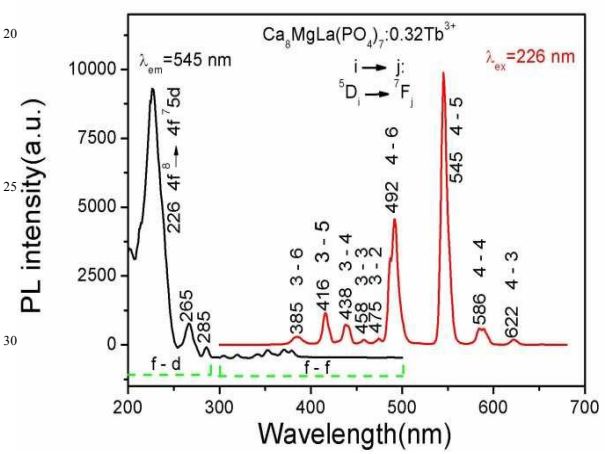

Figure 5. The excitation spectrum and emission spectrum of CMLP:0.32Tb^{3+} sample.

As shown in Figure 6, the excitation spectrum obtained by monitoring at 545 nm ($^5D_4 \rightarrow {}^7F_5$ transition of Tb) including the excitation bands of Ce^{3+} and Tb^{3+}. The excitation spectra in Figure 6 imply an efficient energy transfer from Ce^{3+} to Tb^{3+} in CMLP: 0.02Ce^{3+}, 0.32Tb^{3+}. Figure 7a shows the emission spectra of CMLP: 0.02Ce^{3+}, $x$$Tb^{3+}$ (x =0,…0.98) sample excited by 291 nm UV. The concentration of Ce^{3+} was fixed at 2%, the emission intensity for Ce^{3+} decreased with increasing Tb^{3+} concentration, whereas the emission intensity for Tb^{3+} increases with increases of its concentration. Figure 7b represents the emission spectra of the phosphor CMLP: $y$$Ce^{3+}$, 0.08$Tb^{3+}$ (y = 0.02, …0.07) samples. Although the concentration of Tb^{3+} was fixed at 8%, the emission intensity of Tb^{3+} dramatically increased with increasing Ce^{3+} concentration. All of these results indicate the efficient ET from Ce^{3+} to Tb^{3+}.[39] To further validate the ET from Ce^{3+} to Tb^{3+}, we investigated the lifetimes of Ce^{3+} in the CMLP:0.02Ce^{3+}, $x$$Tb^{3+}$.

As described by Blasse and Grabmaier, the decay behavior of Ce^{3+} can be expressed by:[40,41]

$$I = I_0 \exp(-t/\tau) \qquad (2)$$

Where I and I_0 are the luminescence intensities at time t and

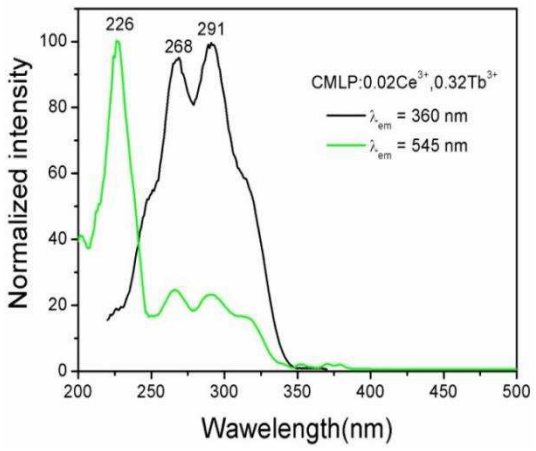

Figure 6. The excitation spectrum of CMLP:0.02Ce^{3+}, 0.32Tb^{3+} sample monitored at 360 nm and 545 nm.

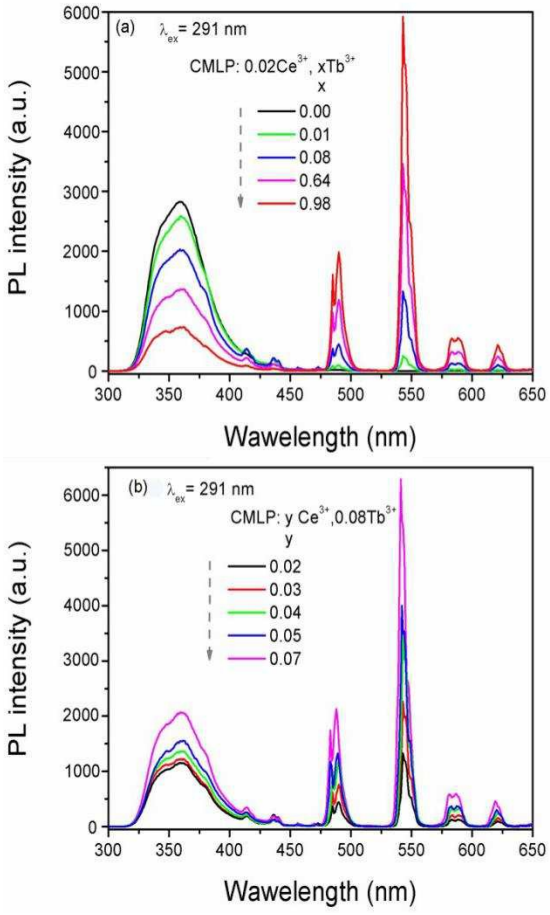

Figure 7. Excitation spectra of CMLP:0.02Ce^{3+}, $x$$Tb^{3+}$ (a) and CMLP:$y$$Ce^{3+}$, 0.08$Tb^{3+}$ (b) under 291 nm UV excitation.

0, and τ is the luminescence lifetime. For the CMLP:0.02Ce^{3+}, $x$$Tb^{3+}$($x$ =0, 0.01, 0.08, 0.64, 0.98) samples, the lifetime of decreases with increasing Tb^{3+} concentration, which is 51.7, 47.37, 40.53, 25.17, 12.85 ns, respectively. As shown in Figure 8a, the luminescence lifetime of Ce^{3+} decreases with increasing Tb^{3+} concentration because the energy transfer from Ce^{3+} to Tb^{3+}. These results are strong evidence for the ET from Ce^{3+} to Tb^{3+}. In

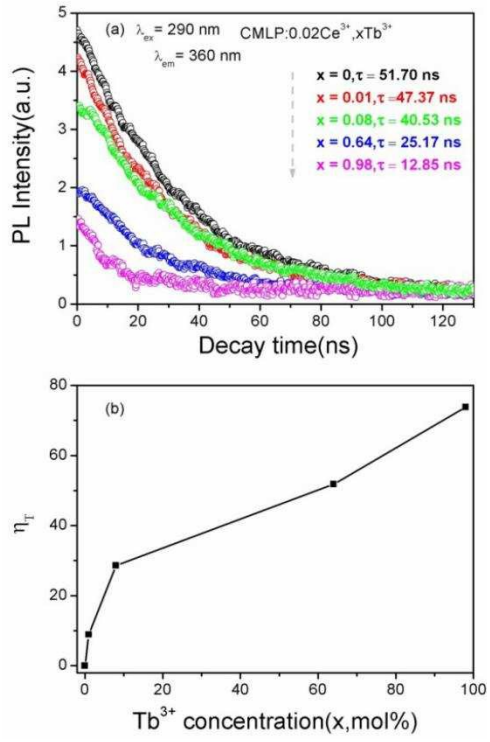

Figure 8. The luminescence lifetime (a) and ET efficiency (b) of CMLP:0.02Ce^{2+}, xTb^{3+} samples.

addition, the ET efficiency from Ce^{3+} to Tb^{3+} was also investigated. Generally, the ET efficiency from sensitizer to activator can be expressed by the following equation:[42,43]

$$\eta = 1 - I_S/I_{S0} \qquad (3)$$

In which η is energy transfer efficiency and I_S and I_{S0} are the luminescence intensities of the sensitizer (Ce^{3+}) with and without the activator (Tb^{3+}) present, respectively. As shown in Figure 8b, luminescence intensities of the sensitizer (Ce^{3+}) decrease with doping concentrations of the activator (Tb^{3+}) increasing, so ET efficiency from Ce^{3+} to Tb^{3+} is found to increase with increasing x. However, the increasing rate of the emission intensity gradually decreases with increasing Tb^{3+} concentration. This result indicates that the ET from Ce^{3+} to Tb^{3+} will tend to saturate with a continuous increase of Tb^{3+} concentration when the Ce^{3+} concentration is fixed. The maximum ET efficiency can reach 74 % under excitation of 291 nm UV. The above results prove that the ET from Ce^{3+} to Tb^{3+} is rather efficient. All of these results indicate the efficient energy transfer from Ce^{3+} to Tb^{3+}. In view of the $Ce^{3+} \rightarrow Tb^{3+}$ transition in the CMLP host, Ce^{3+} ions can strongly absorb UV light from the ground state ($^2F_{5/2}$) to the excited state and then efficiently transfer the energy to the $^5D_3$ level of Tb^{3+} ions; subsequently, the $^5D_3$ level gives its characteristic transitions or continues to transfer the energy to the $^5D_4$ level via cross relaxation, as shown in Figure 9. The absolute quantum yields (56%–71%) and CIE color coordinates of CMLP:0.02Ce^{3+}, xTb^{3+} phosphors under 291 nm UV excitation are summarized in Table 2. Emitting colors of the studied

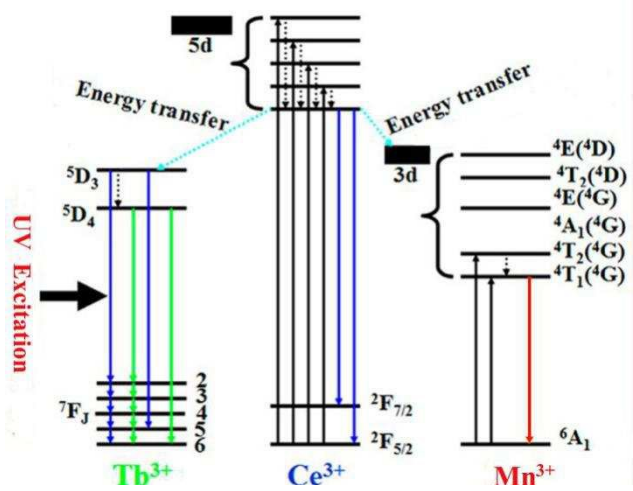

Figure 9. Illustration of the energy-transfer mechanism for Ce^{3+}/Tb^{3+} and Ce^{3+}/Mn^{2+} pairs in the CMLP host.

samples could be adjusted from blue to green via energy transfer and changing concentrations of activated ions. There are main two aspects responsible for the resonant energy-transfer mechanism: one is exchange interaction and the other is multipolar interaction.[44,45] It is known that if energy transfer results from the exchange interaction, the critical distance between the sensitizer and activator should be shorter than 4Å.[45] In many cases, concentration quenching is due to energy transfer from one activator to another until an energy sink in the lattice is reached.[46] The efficiency of energy transfer was calculated by using the concentration quenching method. The critical distance R_{Ce-Tb} between Ce^{3+} and Tb^{3+} can be estimated by the following formula suggested by Blasse:

$$R_C \approx 2\left[\frac{3V}{4\pi X_C N}\right]^{1/3} \qquad (4)$$

Where N is the number of available sites for the dopant in the unit cell, X is the total concentration of Ce^{3+} and Tb^{3+}, V is the volume of the unit cell. For $Ca_8MgLu(PO_4)_7$ host structure, N is 54, and V is 3416.2 Å^3. The critical concentration X_C, at which the luminescence intensity of Ce^{3+} is half of that in the absence of Tb^{3+}, is 0.66. Therefore, the critical distance R_C was calculated to be about 5.7 Å. The radiative emission from Ce^{3+} prevails when $R_{Ce-Tb} > R_C$ and energy transfer from Ce^{3+} to Tb^{3+} dominates when $R_{Ce-Tb} < R_C$. This value is larger than 4Å, indicating little possibility of energy transfer via the exchange interaction mechanism. Hence, the energy transfer from Ce^{3+} to Tb^{3+} ions mainly results from the electric multipolar interaction.[44,45,47]

Based on Dexter's energy transfer formula of multi-polar interaction and Readfield's approximation, the following relation can be obtained:[44,45,47]

$$\frac{\eta_0}{\eta} \propto C_{Ce+Tb}^{n/3} \qquad (5)$$

η_0 and η are the fluorescence quantum efficiencies of the

sensitizer (Ce^{3+}) with and without the activator (Tb^{3+}) present; C is the doping concentration sum of Ce^{3+} and Tb^{3+} ions ; and n= 6, 8, and 10 corresponds to dipole–dipole, dipole–quadrupole, and quadrupole–quadrupole interaction, respectively. η_0/η can be obtained by calculating the luminescent intensity I_{S0}/I_S approximately:[48,49]

$$\frac{I_{S0}}{I_S} \propto C_{Ce+Tb}^{n/3} \qquad (6)$$

Where I_{S0} and I_S are the luminescence intensities of the sensitizer Ce^{3+} with and without activator Tb^{3+} present, respectively.

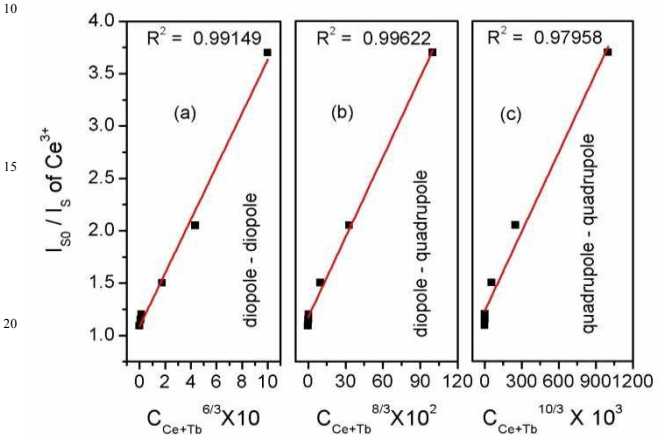

Figure 10. Dependence of I_{S0} /I_S of Ce^{3+} on $C^{6/3}$, $C^{8/3}$ and $C^{10/3}$.

Figure 10 illustrates the relationship between I_{S0}/I_S and $C_{Ce+Tb}^{n/3}$. Only when n is equal to 8, I_{S0}/I_S is approximately linear to the $C_{Ce+Tb}^{n/3}$. This implies that the energy transfer from the sensitizer Ce^{3+} to the activator Tb^{3+} follows a nonradiative dipole-quadrupole mechanism. Therefore, the electric dipole-quadrupole interaction predominates in the ET process from Ce^{3+} to Tb^{3+} ions in the CMLP host. Considering the dipole-quadrupole interaction, the critical distance from the sensitizer to acceptor can also be calculated by the spectral overlap method, as expressed as follows:[47,50]

$$R_C^8 = 3.024\times10^{12}\lambda_S^2 f_q \int \frac{F_S(E)F_A dE}{E^4} \qquad (7)$$

Where f_q is the oscillator strength of the electric quadrupole transition of the acceptor ion (Tb^{3+}) , f_q =$10^{-8.5}$ λ_S (in Å) is the wavelength corresponding to the strongest emission peak of the sensitizer, E is the energy (eV) corresponding to the largest emission wavelength, $\int F_S(E)F_A(E)dE$ represents the spectral overlap between the normalized emission spectrum $F_S(E)$ of the Ce^{3+} and the excitation spectrum $F_A(E)$ of Tb^{3+}, and in our case it is calculated to be about 0.03143 eV^{-4}. The critical distance R_C is calculated to be 5.8 Å by using equation (6). The result agrees approximately with that obtained by using the concentration-quenching method (5.7 Å) and allows us to conclude that the ET mechanism from Ce^{3+} to Tb^{3+} is mainly dipole-quadrupole interaction.

3.2.3 Photoluminescence properties and energy transfer of CMLP: Ce^{3+}, Mn^{2+}

Mn^{2+} ion generally shows a broad band emission because of the $^4T_1 \rightarrow {}^6A_1$ transition within the 3d shell in which the electrons are strongly coupled to lattice vibrations and are affected by crystal field strength and site symmetry. The emission color of Mn^{2+} can vary from green (strong crystal field) to orange/red (weak crystal field).[51,52] Because of the similar electric charges and ionic radius between Mg^{2+} ions and Mn^{2+} ions, Mn^{2+} ions can be doped the crystallographic site 6a to replace Mg^{2+} ions in $Ca_8MgLu(PO_4)_7$.[49] Figure 11 shows the excitation spectrum and emission spectrum of CMLP:0.5Mn^{2+} sample under 406 nm excitation. According to Tanabe-Sugano figure of Mn^{2+} ions, its absorption transitions are both parity-forbidden transition and spin-forbidden transition in the environment of octahedral coordination. Therefore, their excitation transitions are difficult to pump and the emission intensity is very weak. The broad emission band located at 635 nm results from $^4T_1(4G)\rightarrow{}^6A_1(6S)$ transition. Its excitation spectrum includes five absorption band located at 320, 336, 406, 452 and 494 nm, which are corresponding to the absorption of $^6A_1(^6S)\rightarrow{}^4E(^4D)$, $^4T_2(^4D)$, [$^4A_1(^4G)$, $^4E(^4G)$], $^4T_2(^4G)$ and $^4T_1(^4G)$, respectively.[51] The observation of spectral overlap between emission band of Mn^{2+} ions in the CMLP:0.5Mn^{2+} and the excitation band of Ce^{3+} in the CMLP:0.02Ce^{3+} in the Figure 12a, indicates that there is a strong resonant energy transfer between the sensitizer Ce^{3+} ions and the activator Mn^{2+} ions.[27,42]

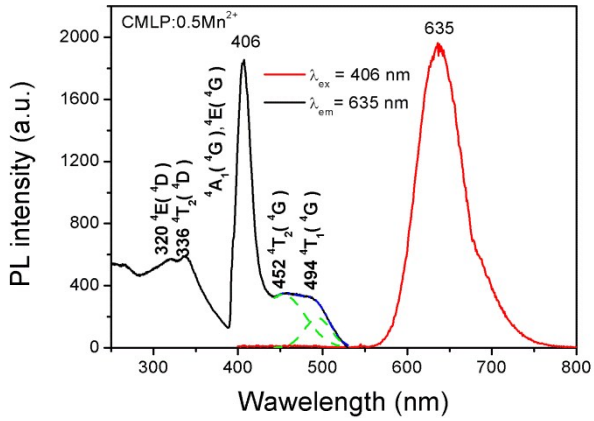

Figure 11. The excitation spectrum and emission spectrum of CMLP: 0.5Mn^{2+} sample.

Figure 12b shows the emission spectra of CMLP:Ce^{3+}, $x$$Mn^{2+}$ sample under 291nm UV excitation. With a fixed concentration of Ce^{3+}, the emission intensity of Ce^{3+} decreased with increasing Mn^{2+} concentration, while the emission intensity of Mn^{2+} increased with the increase of its concentration. It can be observed that the emission intensity of the Mn^{2+} ions reaches maximum at x = 0.6, and then decreases sharply with increasing concentration due to the concentration quenching effect. As shown in Figure 12c, the concentration of Mn^{2+} was fixed, the emission intensity of Mn^{2+} dramatically increased with increasing Ce^{3+} concentration. The above results prove that there is also ET between Ce^{3+} and Mn^{2+}.[53] Similarly, for the CMLP:0.02Ce^{3+}, $x$$Mn^{2+}$ (x =0, 0.05, 0.1, 0.4, 0.6, 1.0) samples, the lifetime of Ce^{3+} decreases with increasing, which is 51.7, 34.1, 24.5, 10.2, 5.1, 2.3 ns, respectively. As shown in Figure 13a, the luminescence lifetime of Ce^{3+} decreases with increasing Mn^{2+} concentration

because the energy absorbed by Ce^{3+} is transferred to Mn^{2+}. These results are strong evidence for the ET from Ce^{3+} to Mn^{2+}. The energy transfer mechanism between sensitizer (Ce^{3+}) and activator (Mn^{2+}) was also calculated by equation (3).

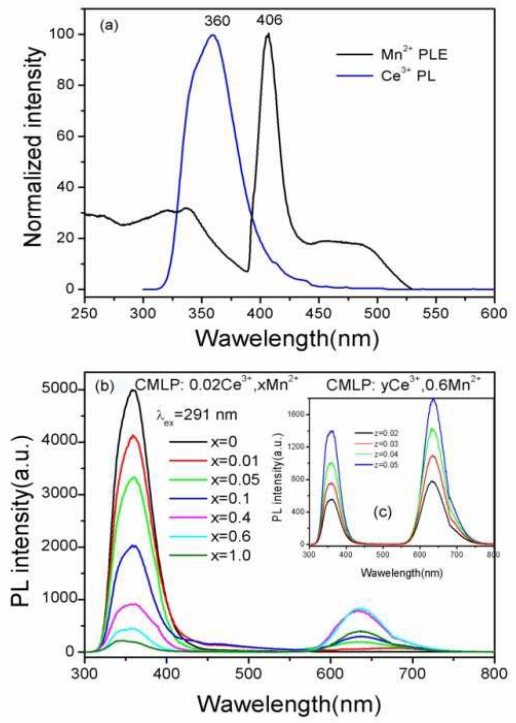

Figure 12. Spectral overlap between the emission spectrum of CMLP: 0.02Ce^{3+} and excitation spectrum of MYS: 0.5Mn^{2+} (a) and the emission spectrum of CMLP: 0.02Ce, $x$$Mn^{2+}$ (b) and CMLP: $y$$Ce^{3+}$, 0.6$Mn^{2+}$ (c) under 291 nm UV excitation.

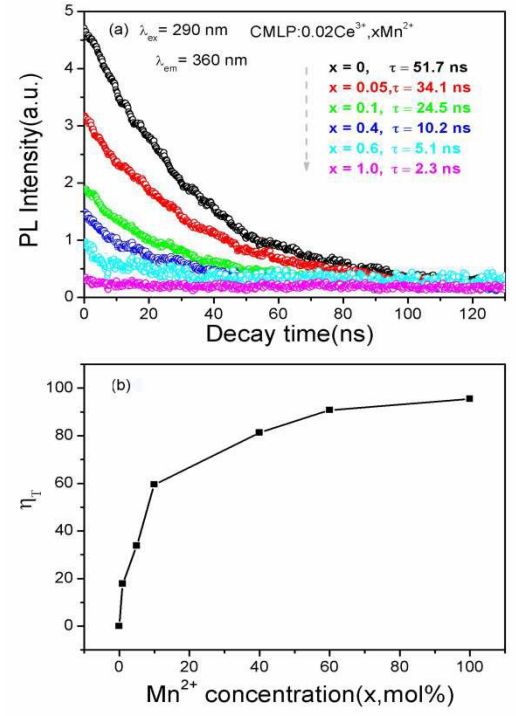

Figure 13. The luminescence lifetime (a) and ET efficiency (b) of CMLP: CMLP: 0.02Ce^{3+}, $x$$Mn^{2+}$ sample.

As shown in Figure 13b, this result indicates that the ET from Ce^{3+} to Mn^{2+} will tend to saturate with a continuous increase of Mn^{2+} concentration when the Ce^{3+} concentration is fixed. The maximum ET efficiency can reach 95% under excitation of 291 nm UV.[20] The above results prove that the ET from Ce^{3+} to Mn^{2+} is rather efficient. The absolute quantum yields (9–56%) of CMLP:Ce^{3+}, Mn^{2+} phosphors under UV excitation are summarized in Table 2. Emitting colors of the studied samples could be adjusted from blue to red via energy transfer interaction and changing concentrations of activated ions.

Figure S1 illustrates the relationship graphics between I_{S0}/I_S and $C_{Ce+Mn}^{n/3}$ when n are equal to 6, 8, 10, respectively. The curve between I_{S0}/I_S and $C_{Ce\text{-}Mn}^{n/3}$ is more close to the linear relation when n= 8 and this clearly manifests that the energy transfer between Ce^{3+} and Mn^{2+} is the dipole–dipole mechanism in CMLP host. The critical distance (R_C) calculated by the quenching concentration method and spectral overlap method are 9.7 Å and 7.9 Å, respectively. (f_q =10^{-10} when Mn^{2+} is the acceptor ion).

3.2.4Luminescent properties of CMLP: Ce^{3+}, Tb^{3+}, Mn^{2+}

It is a feasible method to adjust the illuminant color of CMLP: Ce^{3+}, Tb^{3+}, Mn^{2+} controllably via the energy transfer from sensitizer to activator and achieve white light via controlling certain ratio of activators.[54] Due to the 5d→ 4f transition of the Ce^{3+} ions, the CMLP:Ce^{3+} sample exhibits blue emission and the ETs from Ce^{3+} to Tb^{3+}/Mn^{2+} in the CMLP host have been demonstrated to exist. The ETs from Ce^{3+} to Tb^{3+}/Mn^{2+} in the CMLP host have been demonstrated to exist. So we can achieve white light via adjusting the concentration of Tb^{3+} ions and Mn^{2+} ions with a fixing concentration of Ce^{3+} (sensitizer) in the CMLP host. Our experiment has also confirmed this hypothesis. We synthesize a series of CMLP: 0.02 Ce^{3+}, $x$$Tb^{3+}$, $y$$Mn^{2+}$ samples (x=0, 0.02, 0.03, 0.04, y=0, 0.04, 0.08……0.2) with different concentrations of Tb^{3+} ions and Mn^{2+} ions. Figure 14a-c shows the emission spectrum of CMLP: 0.02 Ce^{3+}, $x$$Tb^{3+}$, $y$$Mn^{2+}$ samples under 291nm UV excitation. With a fixed concentration of Ce^{3+}, the emission intensity of Ce^{3+} decreased with increasing Mn^{2+} and Tb^{3+} concentration, while the emission intensity of Mn^{2+} and Tb^{3+} increased with the increase of their concentration; Similarly, with fixed concentrations of Ce^{3+} and Tb^{3+}, the emission intensity of Ce^{3+} and Tb^{3+} decreased with increasing Mn^{2+} concentration, while the emission intensity of Mn^{2+} increased with the increase of its concentration. Under UV excitation, energy transfers of Ce^{3+}→Tb^{3+}, Ce^{3+}→Mn^{2+}, and Tb^{3+}→Mn^{2+} were observed simultaneously in the CMLP phosphor.[5]

As shown in Figure 14d, with the value of x and y increasing, the chromaticity coordinates of CMLP: 0.02 Ce^{3+}, $x$$Tb^{3+}$ and CMLP: 0.02 Ce^{3+}, $y$$Mn^{2+}$ shifts from blue region to red region (arrow a) and from blue region to green region (arrow b), respectively. More importantly, a white emission of tunable light can be obtained in the certain component samples, such as CMLP:0.02Ce^{3+}, 0.04Tb^{3+}, 0.04Mn^{2+} and CMLP:0.02Ce^{3+}, 0.04Tb^{3+}, 0.08Mn^{2+}, which highest absolute quantum yield can be researched CMLP:0.02Ce^{3+}, 0.04Tb^{3+}, 0.04Mn^{2+}. The absolute quantum yields and CIE color coordinates for CMLP: 0.02Ce^{3+},

Table 2. Absolute Quantum Yields (QYs) and chromaticity coordinates (*x*, *y*) of CMLP:Ce^{3+}, Mn^{2+}, Tb^{3+} samples under 291 nm UV excitation.

Sample	Quantum yields（%）	Quantum yields (*x,y*)
CMLP:0.02Ce^{3+}	56	(0.177,0.086)
CMLP:0.02Ce^{3+},0.01Tb^{3+}	56	(0.192,0.110)
CMLP:0.02Ce^{3+},0.08Tb^{3+}	59	(0.202,0.216)
CMLP:0.02Ce^{3+},0.16Tb^{3+}	65	(0.230,0.413)
CMLP:0.02Ce^{3+},0.64Tb^{3+}	68	(0.247,0.526)
CMLP:0.02Ce^{3+},0.98Tb^{3+}	71	(0.253,0.573)
CMLP:0.02Ce^{3+},0.01Mn^{2+}	47	(0.229,0.137)
CMLP:0.02Ce^{3+},0.05Mn^{2+}	40	(0.251,0.147)
CMLP:0.02Ce^{3+},0.1Mn^{2+}	25	(0.307,0.190)
CMLP:0.02Ce^{3+},0.15Mn^{2+}	21	(0.349,0.215)
CMLP:0.02Ce^{3+},0.4Mn^{2+}	17	(0.476,0.260)
CMLP:0.02Ce^{3+},0.6Mn^{2+}	20	(0.528,0.295)
CMLP:0.02Ce^{3+},1.0Mn^{2+}	9	(0.570,0.319)
CMLP:0.02Ce^{3+},0.02Tb^{3+},0.04Mn^{2+}	44	(0.283,0.226)
CMLP:0.02Ce^{3+},0.02Tb^{3+},0.08Mn^{2+}	27	(0.318,0.237)
CMLP:0.02Ce^{3+},0.03Tb^{3+},0.04Mn^{2+}	45	(0.294,0.249)
CMLP:0.02Ce^{3+},0.03Tb^{3+},0.08Mn^{2+}	30	(0.334,0.250)
CMLP:0.02Ce^{3+},0.04Tb^{3+},0.04Mn^{2+}	50	(0.302,0.280)
CMLP:0.02Ce^{3+},0.04Tb^{3+},0.08Mn^{2+}	35	(0.333,0.275)

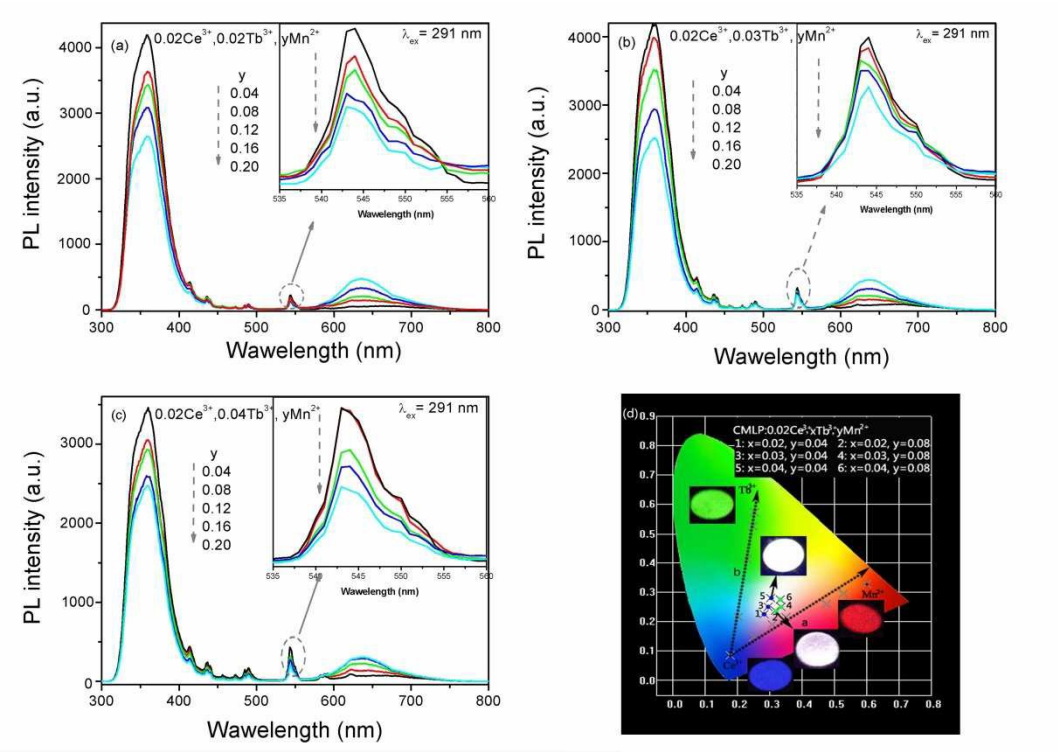

Figure 14. The emission spectrum (a, b, c) and the CIE chromaticity diagram (d) of CMLP:Ce^{3+}, Tb^{3+}, Mn^{2+} sample under 291 nm UV excitation.

xTb^{3+}, *y*Mn^{2+} samples are also summarized in Table 2.

3.3 Temperature quenching effect

Thermal stability is one of the most important factors that should be taken into consideration when preparing phosphors for LEDs. That is because the luminescence intensity for most phosphors would decrease if the operation temperature exceeds some certain value due to temperature quenching effect.[55] Phosphors chosen for LEDs must sustain stable emission efficiency at temperatures of about 150°C over a long term.[56] Figure 15a-b shows the selected temperature-dependent emission spectra of the representative CMLP:0.02Ce^{3+}, 0.64Tb^{3+} and CMLP:0.02Ce^{3+}, 0.6Mn^{2+} sample. The profiles of the emission spectra for the two samples are almost unchanged despite the fact that the temperature increases (T=300-500K). Figure 15c-d plots the temperature-dependent integrated luminescence intensities and CIE chromaticity coordinates of the phosphors. It can be observed that the emission intensity decrease with an increase in temperature. However, the thermal quenching temperatures ($T_{0.5}$, defined as the temperature at which the emission intensity is 50% of its original value) for these two samples are both higher than 500 K (> 227 °C). The results suggest that CMLP:0.02Ce^{3+}, 0.64Tb^{3+} and CMLP: 0.02Ce^{3+}, 0.6Mn^{2+} phosphors have good thermal stability against the temperature quenching effect. In

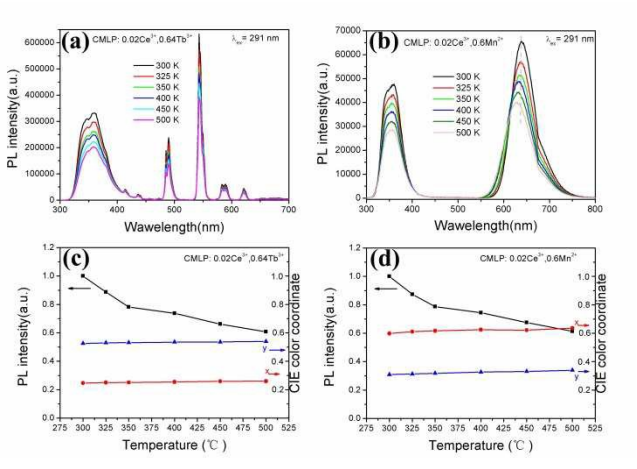

Figure 15. Selected temperature-dependent emission spectra of CMLP:0.02Ce^{3+}, 0.64Tb^{3+} (a) and CMLP:0.02Ce^{3+}, 0.6Mn^{2+} (b) samples and temperature-dependent integrated luminescence intensities (c) and CIE color coordinates (d).

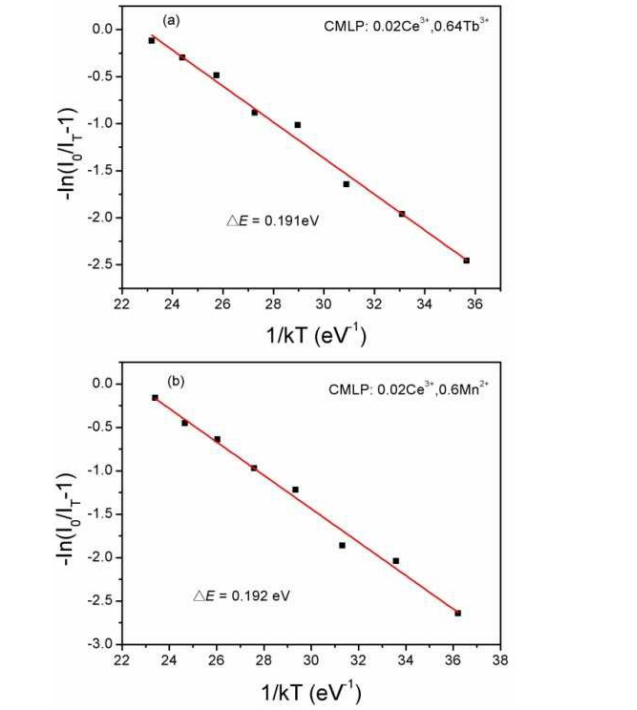

Figure 16. Plots of –ln[(I_0/I_T) -1] versus 1/kT for CMLP:0.02Ce^{3+}, 0.64Tb^{3+} (a) and CMLP:0.02Ce^{3+}, 0.6Mn^{2+} (b) samples.

addition, the emission bands of Mn^{2+} in CMLP:0.02Ce^{3+}, 0.6Mn^{2+} samples show a blue-shift with increasing temperature. A similar phenomenon has been found and studied in other Mn^{2+} ion doped phosphors reported previously.[57,58] The CIE chromaticity coordinates of CMLP:0.02Ce^{3+}, 0.64Tb^{3+} and CMLP: 0.02Ce^{3+}, 0.6Mn^{2+} samples at different temperatures are also illustrated in Figure 15c-d. Clearly, both of samples have good color stability. Additionally, the activation energy ΔE (the energy required to raise the electron from the relaxed excited level to the host lattice conduction band) can be calculated by the following expression:[59-63]

$$I_T = I_0\left[1 + c\exp\left(-\frac{\Delta E}{kT}\right)\right]^{-1} \qquad (8)$$

Where I_0 is the initial emission intensity, I_T is the intensity at temperature T, c is a constant, ΔE is the activation energy (k is the Boltzmann constant, 8.629×10^{-5} eV·K^{-1}). Figure 16a-b shows the plots of -ln[(I_0/I_T) -1] and 1/kT for CMLP:0.02Ce^{3+}, 0.64Tb^{3+} and CMLP:0.02Ce^{3+}, 0.6Mn^{2+} samples. According to equation 8, the activation energy ΔE was calculated to be 0.191eV for CMLP: 0.02Ce^{3+}, 0.64Tb^{3+} and 0.192 eV for CMLP: 0.02Ce^{3+}, 0.6Mn^{2+}.

4. Conclusion

Ce^{3+}, Tb^{3+}, Mn^{2+} ion single/multiple-doped CMLP phosphors have been synthesized by high temperature solid state method. The structure of $Ca_8MgCe(PO_4)_7$ belonging to the family of pyrophosphorite compounds and two types of Ce^{3+} sites in$Ca_8MgCe(PO_4)_7$ are ascertained via GSAS structure refinement method. Under UV excitation, CMLP:Ce^{3+} shows a blue emission with a broad band. The absolute quantum yield of CMLP:0.02Ce^{3+} is 56% and the chromaticity coordinates is (0.177, 0.086). Moreover, with increasing concentrations of Ce^{3+}, the emission peaks appear a red shift in the CMLP host. Both of the ETs from Ce^{3+} to Tb^{3+} and from Ce^{3+} to Mn^{2+} in the CMLP host have been demonstrated to be resonant type via a dipole–quadrupole mechanism. By using the concentration-quenching method, the critical distance R_C from Ce^{3+} to Tb^{3+} and from Ce^{3+} to Mn^{2+} were calculated to be about 5.7 Å and 9.7 Å, respectively. By using the spectral overlap method, the critical distance R_C from Ce^{3+} to Tb^{3+} and from Ce^{3+} to Mn^{2+} were calculated to be about 5.8 Å and 7.9 Å, respectively. The maximum quantum yields of CMLP:Ce^{3+}, Tb^{3+} and CMLP:Ce^{3+}, Mn^{2+} can reach up to 71% and 47%, respectively. The maximum ET efficiency from Ce^{3+} to Tb^{3+} and from Ce^{3+} to Mn^{2+} are 74% and 95%, respectively. The illuminant color of CMLP:Ce^{3+}, Tb^{3+}, Mn^{2+} can be adjusted controllably via the energy transfer and a white emission was observed in the single-component CMLP:0.02Ce^{3+}, $x$$Tb^{3+}$, $y$$Mn^{2+}$ (x=0.02, 0.03, 0.04; y=0.04, 0.08) samples. Moreover, the synthesized samples exhibit good thermal stability. In a word, our results show that the obtained phosphors could be a promising single-component white light-emitting phosphor for UV-converted white LEDs.

Acknowledges

This work is financially supported by the National Natural Science Foundation of China (NSFC 91433110, 51332008, 51472234, 21221061), the Joint Funds of the National Natural Science Foundation of China and Guangdong Province (U1301242), the National Basic Research Program of China (2014CB643803), the Scientific and Technological Department of Jilin Province (grant number 20130522176JH) and the Jilin Postdoctoral Sustentation Fund of China (Grant No. RB201348).

Notes and references

[a]*State Key laboratory of Rare Earth Resource Utilization, Changchun Institute of Applied Chemistry, Chinese Academy of Sciences, Changchun, 130022, China.*

[b]School of Materials Science and Engineering, Changchun University of Science and Technology, Changchun 130022, China

Electronic Supplementary Information (ESI) available: [Figure S1. Dependence of I_{S0} /I_S of Ce^{3+} on $C^{6/3}$, $C^{8/3}$ and $C^{10/3}$]. SeeDOI:10.1039/b000000x/

1 Y. S. Tang and S. F. Hu, *Appl. Phys. Lett*., 2007, **90**(15), 151–108.

2 F. H. Wang, D. Z. Zhou, S. Y. Ma, H. W. Yu and P. L. Li, Z. P. Yang, *J. Alloy. Compd*., 2011, **509**(14), 4824–4826.

3 Y. Liu, X. Zhang, Z. Hao, X. Wang and J. Zhang, *Chem. Commun.*, 2011, **47**, 10677–10679.

4 J. S. Kim, P. E. Jeon, Y. H. Park, J. C. Chol, H. L. Park, G. C. Kim and T. W . Kim, *Appl. Phys. Lett.*, 2004, **85**(17), 3696.

5 D. L. Geng, G. G. Li, M. M. Shang, D. M. Yang, Y. Zhang, Z. Y. Cheng and J. Lin, *J. Mater. Chem.*, 2012, **22**, 14262–14271.

6 J. S. Kim, P. E. Jeon, J. C. Choi, H. L. Park, S. I. Mho and G. C. Kim, *Appl. Phys. Lett.*, 2004, **84**, 2931–2933.

7 Z. L. Fu, X. J. Wang, Y. M. Yang, Z. J. Wu, D. F. Duan and X. H. Fu, *Dalton Trans*., 2014, **43**, 2819–2827.

8 C. K. Chang and T. M. Chen, *Appl. Phys. Lett*., 2007, **90**, 1619011.

9 P. L. You, G. F. Yin, X. C. Chen, B. Yue, Z. B. Huang, X. M. Liao and Y. D. Yao, *Opt. Mater.*, 2011, **33**, 1808.

10 Z. P. Yang, P. F. Liu and L. Lv, *J. Alloys Compd*., 2013, **562**, 176–181.

11 J. C. Zhang, Y. Z. Long, H. D. Zhang, B. Sun, W. P. Han and X. Y. Sun, *J. Mater. Chem. C*, 2014, **2**, 312–318.

12 V. Bedekar, D. P. Duttal, M. Mohapatra, S. V. Godbole, R. Ghildiyal and A. K. Tyagi, *Nanotechnology*, 2009, 20125707.

13 Y. N. Xue, F. Xiao and Q. Y. Zhang, *Spectrochimica. Acta, Part A*, 2011, **78**, 1445–1448.

14 A. Bessiere, R. A. Benhamou, G. Wallez, A. Lecointre and B.Viana, *Acta Mater.*,2012,**60**, 6641–6649.

15 D. W. Wen, Z. Y. Dong, J. X. Shi, M. L. Gong and M. M. Wu, *ECS J. Solid State Sci. Technol.*, 2013, **2** (9), 178–185.

16 H. Yanlin, D. Haiyan, J. Kiwan, C. Eunjin, L. Ho, M. Jayasimhadri and Y. Soung. Soo, *J. Phys. D: Appl. Phys.*, 2008, **41**, 095110.

17 Y. Huang, C. Jiang, Y. Cao, L. Shi and H. J. Seo, *Mater. Res. Bull.*, 2009, **44**, 793.

18 Y. L. Huang, W. X. Zhao, Y. G. Cao, K. W. Jang, Ho. Sueb. Lee, C. Eunjin and Y. Soung. Soo, *J. Solid State Chem.*, 2008, **181**, 2161–2164.

19 C. Larson and R. B. Von Dreele, *General Structure Analysis System (GSAS)*, Los Alamos National Laboratory, Los Alamos, NM, 1994, 86−748.

20 C. C. Zhao, X. Yin, Y. M. Wang, F. Q. Huang and Y. Hang, *J. Lumin.*, 2012, **132**, 617–621.

21 F. P. Du, Y. Nakai, T. Tsuboi, Y. L. Huang and H. J. Seo, *J. Mater. Chem.*, 2011, **21**, 4669–4678.

22 R. A. Benhamou, Au. Bessiere, G. Wallez, B. Viana, M. Elaatmani, M. Daoud and A. Zegzouti, *J. Solid. State. Chem.*, 2009, **182**, 2319–2325.

23 Y. L. Huang, W. X. Zhao, Y. G. Cao, K. W. Jang, Ho. Sueb. Lee, E. J. Cho and S. S. Yi, *J. Solid. State. Chem.*, 2008, **181**, 2161–2164.

24 C. H. Huang, Y. C. Chen, T. M. Chen, T. S. Chan and H. S. Sheu., *J. Mater. Chem*., 2011, **21**, 5645–5649.

25 Y. Q. Li, N. Hirosaki, R. J. Xie, T. Takeda and M. Mitomo, *Chem. Mater.,*2008, **20**, 6704–6714.

26 Van Uitert, L. G, *J. Lumin.*, 1984, **29**, 1–9.

27 Q. Wang, Z. P. Ci, G. Zhu, M. d. Que, S. Y. Xin, Y. Wen and Y. H. Wang, *ECS J. Solid State Sci. Technol.*, 2012, **1**(3), 92–97.

28 I. N. Ogorodnikov, I. N. Sedunova, L. I. Isaenko, S. A. Zhurkov. *Phys. Solid State*, 2012, **54**(3), 485–492.

29 J. Gopaiakrishnan and A. Manthiram, *J. Chem. Soc., Dalton Trans.*, 1981, **3**, 668–672.

30 Z. J. Zhang, X. Lin, Ji. T. Zhao and G.B. Zhang, *Materials Research Bulletin*, 2013, **48**, 224–231.

31 J. Zhao, C. F. Guo, J. Yu and R. J. Yu, *Opt. Laser Technol*., 2013, **45**, 62–68.

32 B. V. Rao, G.S.R. Rayu, I. Omkaram and S. Buddhudu,. *Optoelectron. Adv. Mater-Rapid Commun*., 2008, **2**(1), 17–21.

33 P. Boutinaud, L. Sarakha, R. Mahiou, P. Dorenbos and Y. Inaguma, *J. Lumin*., 2010, **130**, 1725–1729.

34 P. Dorenbos, *Phys. Rev. B.*, 2002, **65**, 235110.

35 P. Dorenbos, *J. Lumin*., 2003, **105**, 117–119.

36 X. Liu, L. Yan and J. Zou, *J. Electrochem. Soc*., 2010, **157**, 1–6.

37 H. L. Li, Z. L. Wang, S. J. Xu and J. H. Hao, *J. Electrochem. Soc*., 2009, **156**, J112–J116.

38 K. S. Sohn, Y. Y Choi, H. D. Park and Choi. H. G, *J. Electrochem. Soc.*, 2000, **147**, 2375-2379.

39 Q. Zhang, J. Wang, G. Zhang and Q. Su, *J. Mater. Chem*., 2009, **19**, 7088–7092.

40 S. Neeraj, N. Kijima and A. K. Cheetham, *Solid State Commun*., 2004, **131**, 65–69.

41 L. L. Han, Y. H. Wang, J. Zhang and Y. Z. Wang, *Mater. Chem. Phys*., 2013, **139**, 87–91.

42 P. I. Paulose, G. Jose, V. Thomas, N. V. Unnikrishnan and K. R. M. Warrier, *J. Phys. Chem. Solids*, 2003, **64**, 841-846.

43 R. Reisfeld, E. Greenberg, R. Velapoldi and B. Barnett, *J. Chem. Phys*., 1972, **56**, 1698-1706.

44 B. M. Antipeuko, I. M. Bataev, V. L. Ermolaev, E. I. Lyubimov and T. A. Privalova, *Opt. Spectrosc.*, 1970, **29**, 177.

45 D. L. Dexter and J. A. Schulman, *J. Chem. Phys.*, 1954, **22**, 1063–1071.

46 G. Blasse, *Philips Res. Rep.*, 1969, **24**, 131–134.

47 H. P. You, J. L. Zhang, G. Y. Hong and H. J. Zhang, *J. Phys. Chem. C*, 2007, **111**, 10657–10661.

48 C. C. Lin, R. S. Liu, Y. S. Tang and S. F. Hu, *J. Electrochem. Soc.*, 2005, **155**, 248–251.

49 K. H. Kwon, W. B. Im, H. S. Jang, H. S. Yoo and D. Y. Jeon, *Inorg. Chem.*, 2009, **48**, 11525–11532.

50 N. Guo, Y. J. Huang, H. P. You, M. Yang, Y. H. Song, K. Liu and Y. H. Zheng, *Inorg. Chem.*, 2010, **49**, 10907–10913.

51 G. Blasse and B. C. Grabmarier, *Luminescent Materials; Sprinnger-Verlag: Berlin, Germany,* 1994, **18**, p96.

52 L. Shi, Y. L. Huang and H. J. Seo, *J. Phys. Chem. A*, 2010, **114**, 6927–6934.

53 C. H. Huang, T. W. Kuo and T. M. Chen, ACS. *Appl. mat. interfacses*, 2010, **2**(5), 1395–1399.

54 G. G. Li, D. L. Geng, M. M. Shang, Y. Zhang, C. Peng, Z. Y. Cheng and J. Lin, *J. Phys. Chem. C*, 2011, **115**, 21882–21892.

55 D. Dutczak, C. Ronda, A .Meijerink and T .Justel, *J. Lumin.*, 2013, **141**, 150–154.

56 C. W. Yeh, W. T. Chen, R. S. Liu, S. F. Hu, H. S. Sheu, J. M. Chen and H. T. Hintzen, *J. Am. Chem. Soc.*, 2012, **134**, 14108–14117.

57 X. Zhang and M. Gong, *Mater. Lett.*, 2011, **65**, 1756–1758.

58 D. Geng, M. Shang, D. Yang, Y. Zhang, Z. Cheng and J. Lin, *J. Mater. Chem.*, 2012, **22**, 23789-23798.

59 Y. Huang, J. Gan, R. Zhu, X. Wang and H. J. Seo, *J. Electrochem. Soc*., 2011, **158**, 334–340.

60 Y. Huang, Y. Nakai, T. Tsuboi and H. J. Seo, *Opt. Express*, 2011, **19**, 6303–6311.

61 W. R. Liu, C. W. Yeh, C. H. Huang, C. C. Lin, Y. C. Chiu, Y. T. Yeh and R. S. Liu, *J. Mater. Chem.*, 2011, **21**, 3740–3744.

62 L. Chen, C. C. Lin, C. W. Yeh and R. S. Liu, Materials, 2010, **3**, 2172–2195.

63 D. L. Geng, M. M. Shang, Y. Zhang, Z. Y. Cheng and J. Lin. *Eur. J. Inorg. Chem.*, 2013, 2947–2953.

TOC

With the value of *x* and *y* increasing, the chromaticity coordinates of CMLP: 0.02 Ce^{3+}, *x*Tb^{3+} and CMLP: 0.02 Ce^{3+}, *y* Mn^{2+} shifts from blue region to red region(arrow a) and from blue region to green region (arrow b), respectively. More importantly, a white emission of tunable light can be obtained in the certain component samples, such as CMLP: 0.02Ce^{3+}, 0.04Tb^{3+}, 0.04Mn^{2+} and CMLP: 0.02Ce^{3+}, 0.04Tb^{3+}, 0.08Mn^{2+}, which highest absolute quantum yield can be researched CMLP: 0.02Ce^{3+}, 0.04Tb^{3+}, 0.04Mn^{2+}.